Y. Xu, *et al.*, Study on the Wall Backscatter Factor in Mobile X-Ray *In-Situ* Calibration
Nuclear Technology & Radiation Protection: Year 2024, Vol. 39, No. 4, pp. 270-279

270

STUDY ON THE WALL BACKSCATTER FACTOR IN MOBILE X-RAY *IN-SITU* CALIBRATION

by

Yang XU [1,2], *Chen LUO* [2], *Yan HUANG* [2*], *Kebin JIA* [1], *Yuntao LIU* [3], *and Min LIN* [3*]

[1] Department of Information and Communication Engineering,
Faculty of Information Technology, Beijing University of Technology, Beijing, China
[2] Division of Electromagnetic Information and Satellite Navigation, Beijing Institute of Metrology, Beijing, China
[3] Division of Radiation Metrology, China Institute of Atomic Energy, Beijing, China

This article focuses on the in-situ calibration of area radiation monitors by examining changes in backscatter factors. A mobile X-ray irradiation device was developed, and a reference radiation level was established. Using the Monte Carlo method, an in-situ calibration measurement model was created to study backscatter factors at different distances and radiation field conditions for radiation qualities ranging from N-60~N-200. The accuracy of the simulation was verified, with a relative deviation between simulation and experimental results not exceeding ±4.7 %. In addition, the variation of the backscatter factors with different chamber-wall distances and wall materials was simulated. Results indicate that backscatter factors for all materials decrease as the chamber-wall distance increases. For conventional concrete, the maximum backscatter factor within the studied energy range did not exceed 1.35. It is important to note that for heavy concrete and lead, the presence of *K* absorption edges can result in a sudden increase in scattered radiation.

Key words: mobile X-ray device, in-situ calibration, air kerma, backscatter factor, Monte Carlo

INTRODUCTION

Nuclear power plants, accelerators, and radiation environment monitoring stations utilize numerous fixed X- and gamma-ray radiation dosimeters. These devices are used for area radiation monitoring, online evaluation, and early warning of radioactive hazards associated with nuclear facilities [1-4]. Considering the accuracy of monitoring, the capability of dosimeters with high sensitivity and quick response are usually required. The conventional method for users to ensure the reliability of measurement results of such fixed radiation dosimeters is to regularly disassemble them from the surface of the installation wall every year and transport them to the primary standard dosimetry laboratories or secondary standard dosimetry laboratories for calibration [5-7]. This method has drawbacks, including cumbersome instrument disassembly, lengthy submission cycles, and the risk of losing control of monitored points during submission. According to the standard IEC 60846-1:2009 [8], the conventional monitoring quantity of the dosimeter is the ambient dose equivalent $H^*(10)$ or air kerma K_a.

The radiation performance mainly evaluates its systematic error, measurement repeatability, and energy response characteristics. Narrow-spectrum series (N-series) filtered X reference radiation or ^{60}Co, ^{137}Cs and ^{241}Am radionuclide gamma reference radiation can be used in calibration. The calibration factor of a dosimeter is defined as *the quotient of the conventional true value of the monitoring quantity by the indicated value (with necessary corrections) of the dosimeter*. It can be seen that the accuracy of the conventional true value measurement at the test post will greatly affect the accuracy of the calibration factor. The ISO 4037-1:2019 indicates that the contribution due to scattered radiation in the fixed reference radiation field should be less than 5 % of the total dose rate at the test point. However, different from the standard laboratory, *in-situ* calibration requires special consideration of the impact of scattered radiation generated by the surrounding environment on the dose rate at the test point.

During *in-situ* calibration, scattered radiation is affected by the installation wall of fixed dosimeters, and by obstacles on the wall surface (such as pipelines, junction boxes, and hosts that are compatible with dosimeter probes). Usually, these obstacles are small in volume and positioned outside the radiation field,

___
* Corresponding authors, e-mails: minlin716@126.com,
huangy@bjjl.cn

hence the dose rate at the test point is less affected by the scattered radiation from these obstacles. In contrast, during the *in-situ* calibration, almost all the radiation fields are perpendicular to the installation wall, resulting in a larger exposed area and a greater interaction probability between the incident X-ray and the wall. The installation position of the dosimeters is usually close to the wall surface, and the backscattered radiation generated by the wall may seriously affect the dose rate of the test point, resulting in significant deviation in the calibration factor measurement results. Therefore, it is important to determine the impact of backscattered radiation from the fixed dosimeter installation wall on the dose rate at the test point when in-situ calibration is adopted. In summary, the backscattered radiation is mainly related to the radiation quality, field size, wall material, and the distance between the dosimeter and the wall.

In this study, a mobile X-ray irradiation device was developed for *in-situ* calibration, and its radiation characteristics were systematically verified according to the standard ISO 4037 [9]. Monte Carlo simulation and experimental methods were used to evaluate the changes in backscattered radiation of the installation wall under different distances, radiation fields, and wall materials. The results provide important references for *in-situ* calibration using mobile X-ray irradiation devices.

THEORY AND METHODS

Establishment of mobile X-ray reference radiation

The reference radiation field generated by the mobile X-ray irradiation device is used to carry out in-situ calibration of the fixed dosimeters, which the typical layout is shown in fig. 1. An XPO EVO 225D portable X-ray tube (YXLON International GmbH) serves as the X-ray source with a 20° tungsten target and a maximum power of 1200 W. The tube voltage ranges from 25 kV to 225 kV (1 kV/step), and the tube current ranges from 0.5 mA to 10 mA (0.1 mA/step). The device features a collimation design, using 2 mm lead and 1 mm stainless steel shielding around the tube to reduce the impact of leakage radiation on the measurement. These dosimeters are mounted on movable support platforms, eliminating the need to remove them from the installation wall during the *in-situ* calibration. The laser positioning module ensures that the X-ray tube focal spot is at the same horizontal height as the calibrated dosimeter reference point and that the central axis of the X-ray beam is perpendicular to the installation wall.

In backscattered radiation measurement, the calibrated dosimeter reference point is replaced by the geometric center of TW 32005 (PTW) secondary standard ionization chamber, the vertical height of the test point is 150 cm and remained unchanged in the following discussion. The distance from the X-ray focal spot to the chamber (SCD) varies from 100 cm to 300 cm, which is commonly used. The distance from the chamber to the installation wall (CWD) ranges from 2.2 cm to 50 cm, with 2.2 cm chosen as it corresponds to the radius of the TW 32005 chamber. Three different sizes of apertures that can respectively adjust the output X-ray to conical beams with angles θ of 5°, 8°, and 10°. For a specific SCD, the radiation field will become larger when θ is increased. According to the dimensions of common fixed dosimeters, beams with an angle θ of 8° are most suitable for *in-situ* calibration, and circular radiation fields with radii r of 14 cm, 28 cm, and 42 cm (including penumbra area) can be obtained at distances of 100 cm, 200 cm, and 300 cm from the focal spot, respectively. Laser locator 1 is

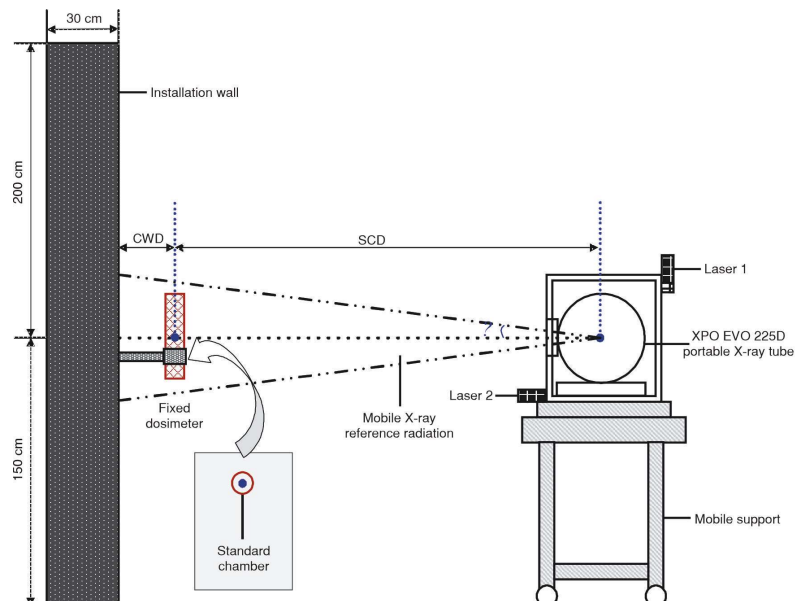**Figure 1. Typical layout for *in-situ* calibration using mobile X-ray irradiation device**

272

Y. Xu, *et al.*, Study on the Wall Backscatter Factor in Mobile X-Ray *In-Situ* Calibration
Nuclear Technology & Radiation Protection: Year 2024, Vol. 39, No. 4, pp. 270-279

Table 1. Characteristics of reference radiation quality

Radiation quality	Tube voltage [kV]	Additional filtration [mm]			Mean energy [keV]	HVL_{st} (in mm Cu)
		Pb	Sn	Cu		
N-60	60	–	–	0.77	48.08	0.24
N-80	80	–	–	1.97	65.40	0.59
N-100	100	–	–	4.94	83.14	1.15
N-120	120	–	1.01	5.02	100.63	1.75
N-150	150	–	2.49	–	119.03	2.43
N-200	200	1.16	3.10	2.03	167.99	4.18

used for spatial alignment between the focal spot and the test point, while laser locator 2 ensures that the field is perpendicular to the installation wall.

Table 1 shows the characteristics of reference radiation qualities used in this paper. The additional filtrations are made of Pb, Sn, and Cu sheets with a purity better than 99.9 %. According to the measurement results, the inherent filtration of the irradiation device is 4.01 mm Al [10]. The calibrated ionization chamber and type UNIDOS E electrometer are used to measure the dose rate at the test point, where the impact of scattered radiation from the surrounding environment can be ignored (that is, the dose rate in free air), and the value is traceable to the primary standard of 60-250 kV X-ray air kerma.

Monte Carlo simulation

Monte Carlo N-Particle Transport Code (MCNP), Version 5 [11] is used for the simulation of backscattered radiation. The MCNP is a general-purpose, continuous-energy, generalized-geometry, time-dependent, coupled neutron/photon/electron Monte Carlo transport code. Figure 2 shows the MCNP model for backscattered radiation calculation, which reproduces the geometric structure of the in-situ calibration experiment in fig. 1. A point source with N-series photon fluence spectra is set up at the focal spot of the X-ray tube, and the source terms used in the
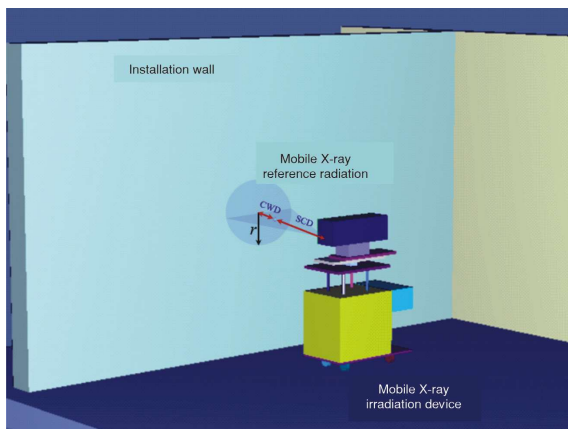

Figure 2. The MCNP calculation model for backscattered radiation

simulation are shown in fig. 3. Figure 3(a) shows the corresponding bremsstrahlung spectra, which is obtained from the calculation model of cathode electron beam bombard to 20° anode tungsten target. By incorporating additional filtration consistent with the material and thickness specified in tab. 1, the *N*-series photon fluence spectra are obtained, as shown in fig. 3(b). Using a DIR card the beam is shaped into a conical form. It is then further adjusted with a beam aperture, ensuring the simulated field range remains consistent with the actual measurement.

A spherical cell with a radius of 2.2 cm is used to simulate the sensitive volume of the transfer chamber. Using an F4 tally card to record the incident photons flux, and its physical quantity is as follows

$$\overline{\phi}_V = \frac{1}{V}\int dE \int dt \int dV \int d\Omega \psi(\vec{r}, \Omega, E, t) \qquad (1)$$

where $\overline{\phi}_V$ is the average flux in spherical tally cell (particles-cm^{-2}), V [cm^3] – the volume of the tally cell, E – the energy of photons incident on the tally cell, $\vec{r}$ [cm] – the particle position vector , Ω – the direction vector, t – time in shake (1 shake = 10^{-8} s), and ψ – the angular flux familiar from nuclear reactor theory. Then, a DE/DF card is used to convert flux into air kerma. The ICRP Report 74 [12] provides the conversion coefficient K_a/ϕ [pGy·cm^2] of air kerma per unit flux, which is a function of incident photon energy.

In this paper, conventional concrete was first chosen as the simulation scattered material, which was commonly used in laboratory wall construction. In the simulation, the dimensions of the fixed dosimeter installation wall were set to 600 cm × 350 cm × 30 cm (*i.e.*, length × height × thickness). These measures remained unchanged. The CWD was set to 4 cm, and SCD was sequentially set to 96 cm and 200 cm. The tube voltage range was adjusted within the range of 60-200 kV, corresponding to radiation qualities N-60~N-200. The simulated values were compared with the measured results to verify the validity of the MCNP model and calculation method. Subsequently, to comprehensively evaluate the backscattered radiation variation in conventional concrete materials, the variation ranges for CWD and SCD were set to 2.2-50 cm and 100-300 cm, respectively. These ranges, commonly used in *in-situ* calibration, were selected to study the variation of the backscattered radiation factor with CWD and SCD. In addition to conventional concrete, brick, heavy concrete, iron, and lead were also employed as simulation scattered materials. The reasons are that brick is used as construction material, iron is used as holder material for fixed dosimeters, and heavy concrete and lead are commonly used as radiation shielding materials. The detailed simulation parameter information of the above five materials is listed in tab. 2, and the relevant data is sourced from the report published by Williams, [13].

Y. Xu, *et al.*, Study on the Wall Backscatter Factor in Mobile X-Ray *In-Situ* Calibration
Nuclear Technology & Radiation Protection: Year 2024, Vol. 39, No. 4, pp. 270-279

273

Figure 3. Source terms used in the backscattered radiation simulation; (a) bremsstrahlung spectra and (b) N-series photon fluence spectra
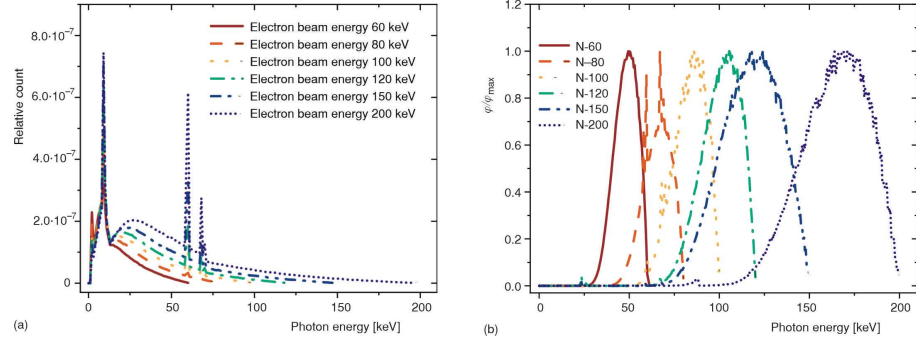
Table 2. Simulation parameters of five materials in *in-situ* calibration

Wall material	Composition information			Density [gcm^{-3}]
	Element	Atomic number (Z)	Weight fraction [%]	
Brick	O	8	52.50	1.800
	Al	13	0.50	
	Si	14	44.90	
	Ca	20	1.40	
	Fe	26	0.70	
Conventional concrete	H	1	0.40	2.180
	O	8	48.21	
	Na	11	0.22	
	Mg	12	1.41	
	Al	13	6.94	
	Si	14	27.75	
	K	19	1.30	
	Ca	20	8.02	
	Fe	26	5.75	
Heavy concrete	H	1	0.36	3.350
	O	8	31.16	
	Mg	12	0.12	
	Al	13	0.42	
	Si	14	1.04	
	S	16	10.79	
	Ca	20	5.02	
	Fe	26	4.75	
	Ba	56	46.34	
Iron	Fe	26	100.00	7.874
Lead	Pb	82	100.00	11.350

Calculation method for backscatter factor

To quantitatively discuss the impact of backscattered radiation from the installation wall on the dose at the test point under different CWD and SCD, we introduced a backscatter factor.

For experimental measurement, the backscatter factor k_{ME} is calculated as follows

$$k_{ME} = \frac{D_{ME}}{D_{ME0}} \qquad (2)$$

where D_{ME0} [mGyh^{-1}] is the dose rate at the test point in free air, and D_{ME} [mGyh^{-1}] – the dose rate at the test point with installation wall backscattered radiation.

For simulation calculation, the backscatter factor k_{MC} is calculated as follows

$$k_{MC} = \frac{D_{MC}}{D_{MC0}} \qquad (3)$$

where D_{MC0} [pGy] is the dose at the tally cell when the installation wall is filled with air and D_{MC} [pGy] – the dose at the tally cell when the installation wall is filled with conventional concrete, heavy concrete, brick, iron, and lead [pGy].

It should be noted that for MCNP simulation, adjusting the tube voltage can be accomplished by setting photon source terms with different spectrum distributions. However, adjusting the tube current cannot be simply achieved by changing the number of photon transports. Increasing the number of photon transports will only reduce the statistical fluctuations of the simulation results. This means that with N different tube currents, N measured backscatter factors k_{ME} will be generated, corresponding to only one simulated backscatter factor k_{MC}. The current of the X-ray tube is proportional to the intensity of the photon source. For a specific energy spectrum distribution, when the output of the X-ray tube is stable, there is no significant change in the backscatter factor, which has been studied [14]. Therefore, in the following discussion, we will ignore the description of tube current.

RESULTS AND DISCUSSION

Experimental verification of backscattered radiation calculation model

The backscattered radiation experiment was carried out in the laboratory of the China Institute of Atomic Energy, and the laboratory wall material was conventional concrete. The statistical uncertainty of the simulation results is less than 2 % (the number of photon histories is set to 10^8). The comparison between k_{ME} and k_{MC} at beam angles θ of 5°, 8°, and 10° for SCD = 96 cm and 200 cm, is shown in fig. 4(a) and fig. 4(b).

In fig. 4(a), the radiation field radius (r) projected at the installation wall changes from 8.5 cm (θ of 5°) to 17 cm (θ of 10°). The interaction probability between in-

274

Y. Xu, *et al.*, Study on the Wall Backscatter Factor in Mobile X-Ray *In-Situ* Calibration
Nuclear Technology & Radiation Protection: Year 2024, Vol. 39, No. 4, pp. 270-279
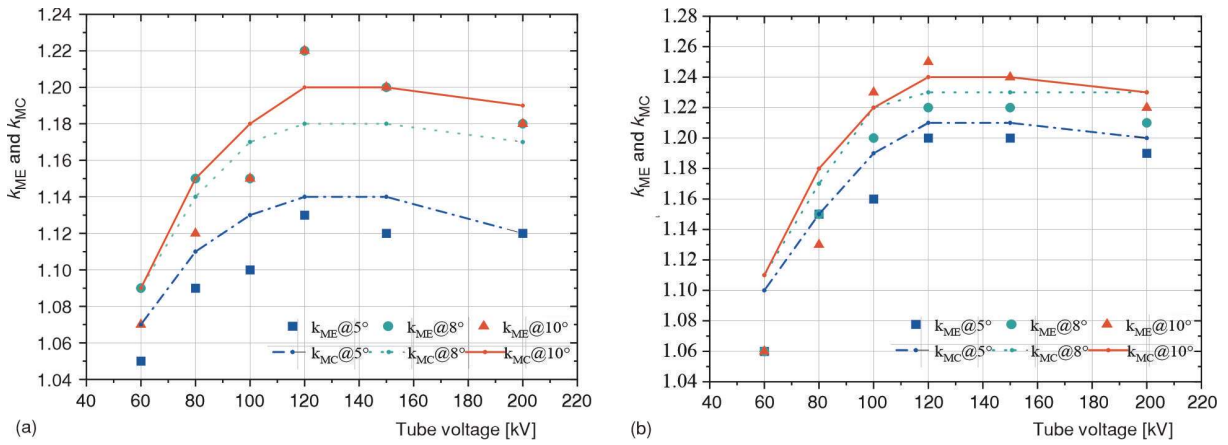
Figure 4. The CWD of 4 cm, θ of 5°, 8°, and 10°, the comparison of k_{ME} and k_{MC} when; (a) SCD of 96 cm, (b) SCD of 200 cm

cident photons and the wall will increase, leading to an increase in backscattered radiation. The k_{ME} changes from 1.13 (θ of 5°) to 1.22 (θ of 10°) when tube voltage is 120 kV, and a similar pattern can also be seen in fig. 4(b). When θ remains unchanged (taking 10° as an example), adjusting the SCD from 96 cm to 200 cm will also increase the radiation filed radius, and the k_{ME} changes from 1.22 (SCD of 96 cm) to 1.25 (SCD of 200 cm) when tube voltage is 120 kV. The relative deviation between the simulated and measured results in fig. 4 is within ±4.7 %, which verifies the validity of the backscattered radiation calculation method and the MC model.

The variation of backscatter factor with CWD

The validated backscattered radiation MC calculation model was used to study the variation of the backscatter factor of conventional concrete walls with CWD under different tube voltages. The beam angle θ was set to 8°, SCD was sequentially set to 100 cm, 200 cm, and 300 cm, and the calculation results are shown in fig. 5.

As shown in fig. 5, the backscatter factor k_{MC} decreased with the increase of CWD and gradually ap-
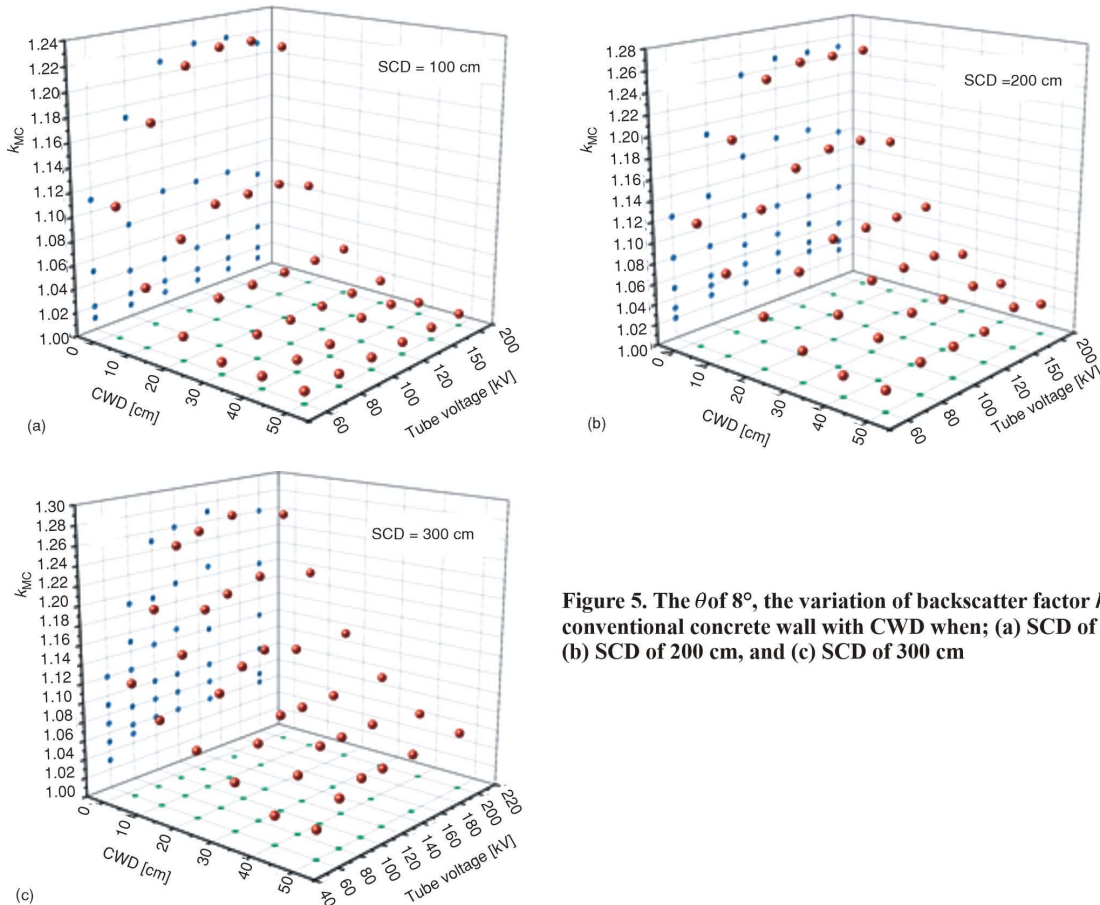

Figure 5. The θ of 8°, the variation of backscatter factor k_{MC} of conventional concrete wall with CWD when; (a) SCD of 100 cm, (b) SCD of 200 cm, and (c) SCD of 300 cm

Y. Xu, *et al.*, Study on the Wall Backscatter Factor in Mobile X-Ray *In-Situ* Calibration
Nuclear Technology & Radiation Protection: Year 2024, Vol. 39, No. 4, pp. 270-279

275

proached 1.00. As the wall gradually moves away, the influence of backscattered radiation on the dose at the test point will gradually decrease and eventually disappear (when the distance is far enough). At CWD of 50 cm, the backscatter factor can be reduced to below 1.01 when SCD is 100 cm, while at SCD of 200 cm and 300 cm, due to the increase of radiation field size, the backscatter factor can only be reduced to below 1.04 and 1.06, respectively. Due to the long distance between the wall and the test point, the fluctuation of the backscatter factor with the tube voltage is small. On the contrary, when the wall is adjacent to the test point (CWD of 2.2 cm), the backscattered radiation will be more easily detected. As the SCD increases from 100 cm to 300 cm, the maximum backscatter factor can increase to 1.22, 1.25, and 1.27, respectively. At this time, the fluctuation of the backscatter factor with the tube voltage is greater than that at CWD of 50 cm.

The aforementioned studied the variation of the backscatter factor at the test point when the wall material is conventional concrete under a commonly used *in-situ* calibration layout. During the *in-situ* calibration, the radiation field size can be reasonably selected based on the actual situation, and the impact of scattered radiation can be reduced by adjusting the measurement distance or the beam aperture size.

The variation of backscatter factor with wall material

The installation wall was sequentially filled with brick, ordinary concrete, heavy concrete, iron, and lead materials, and the variation of backscatter factor k_{MC} with CWD was simulated and the results are shown in fig. 6. The beam angle θ was set to 8°, radiation quality was set to N-60 and N-200, SCD was set to 100 cm and 300 cm, and CWD was set to 2.2-50 cm.

In fig. 6, the backscatter factor k_{MC} of all materials decreases and approaches 1.00 with the increase of CWD, which is consistent with fig. 5. When the wall is adjacent to the test point (CWD of 2.2 cm) and SCD was set to 100 cm, backscatter factors of the five materials under radiation quality N-60 in descending order are: heavy concrete (1.48), lead (1.17), brick (1.16), ordinary concrete (1.11), and iron (1.09). However, backscatter factors of the five materials under radiation quality N-200 in descending order are: brick (1.24), ordinary concrete (1.21), lead (1.09), iron (1.09), and heavy concrete (1.05). The backscatter factors for heavy concrete and lead at N-60 are approximately 41.0 % and 7.3 % higher, respectively, compared to those at N-200. In contrast, the backscatter factors for brick and ordinary concrete at N-60 are about 6.5 % and 8.3 % lower, respectively, than those at N-200. The backscatter factor for iron remains almost unchanged. When SCD was set to 300 cm, a similar pattern can be observed.

Because the reaction cross-section is related to the incident photon energy and the material type, the backscatter factor varies with the radiation quality. Under the X-ray energy of 200 keV, the main forms of interaction of photons with matter include photoelectric absorption, Compton scattering and coherent scattering. The NIST XCOM photon cross-section database provides detailed data on the reaction cross sections of the above five materials [15], as shown in fig. 7. In addition, the X-ray fluence spectra of N-60~N-200 are also shown to characterize the relative weights of different reaction cross sections under different energy photon.

Combining the backscatter factor in fig. 6 with the reaction cross-section in fig. 7, we can see that for brick material, when the photon energy is 20-50 keV, the photoelectric absorption cross-section is larger than the Compton scattering section. When the photon energy ranges from 50-200 keV, the photoelectric absorption cross-section decreases rapidly and Compton scattering gradually becomes dominant. For conventional concrete material, the variation is similar to that of brick, and the cross-section of photoelectric absorption and Compton scattering of these two materials are almost the same near 60 keV. Therefore, for brick and conventional concrete materials, the backscatter factor at N-60 is smaller than at N-200.

For heavy concrete and lead materials, photoelectric absorption is always dominant within the photon energy range of 20-200 keV, mainly because the effective atomic number Z of the material is large, and the probability of photoelectric effect is proportional to the Z^5. However, the barium (mass fraction 46.34 %) in heavy concrete has a K absorption edge at the photon energy of 37.44 keV. For N-60, more characteristic X-rays will be detected, resulting in a sharp increase in the backscatter factor. Similarly, for lead material, there is a K absorption edge at the photon energy of 88.00 keV, which directly leads to a sudden increase of backscatter factor under N-100 and N-120, as shown in fig. 8.

Based on the above analysis of the changes in backscatter factors of five materials under different energy photons, it can be concluded that in the actual calibration process, the main material of the fixed dosimeter installation wall should be fully considered. According to the radiation quality and energy range used in the calibration, it is necessary to consider the sudden change near the K absorption edge on the backscatter factor.

CONCLUSIONS

In this study, a mobile X-ray irradiation device was developed, and reference radiation levels ranging from N-60~N-200 were established. A Monte Carlo model for backscattered radiation calculation was built and validated. The variation of the fixed
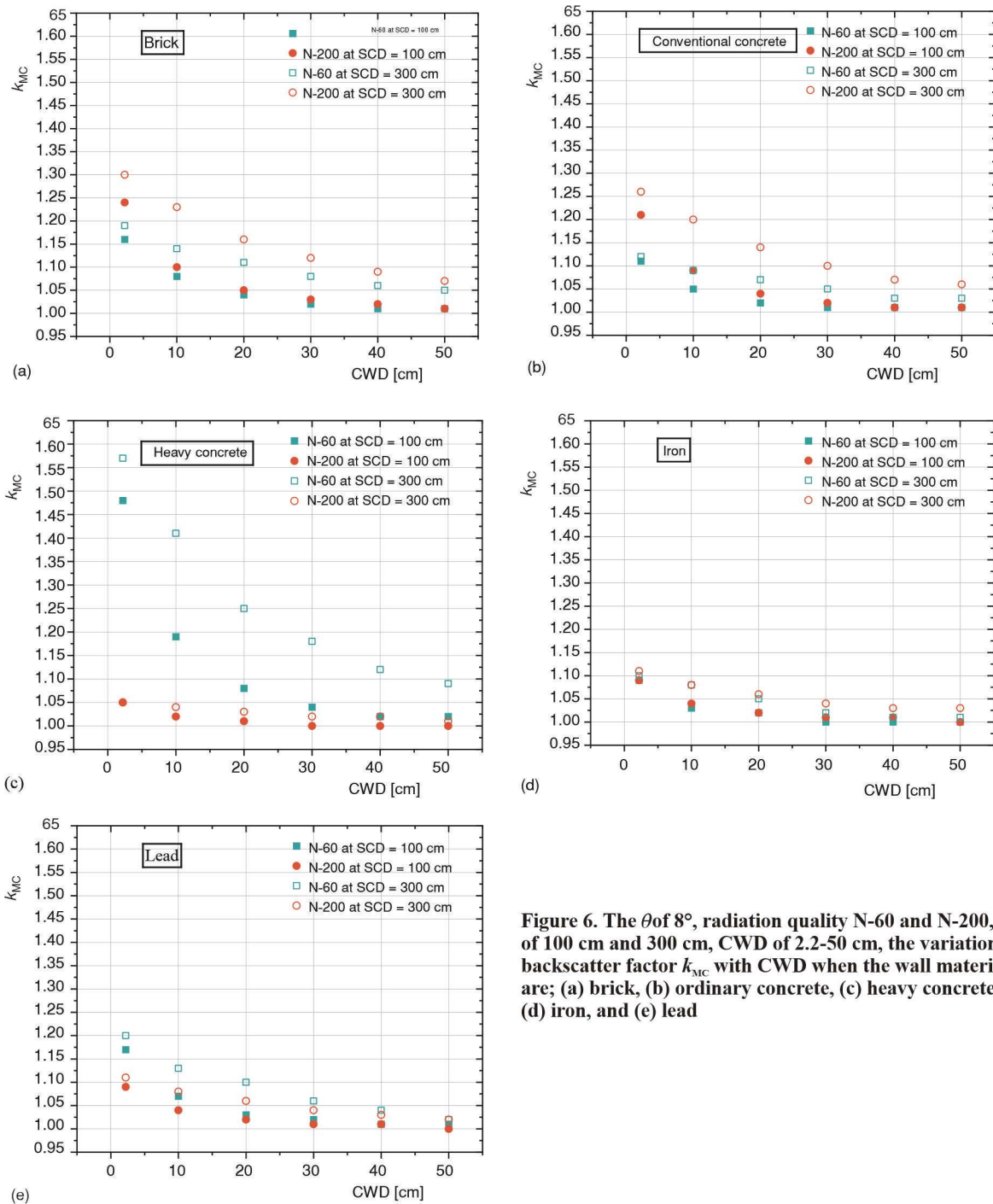
Figure 6. The θ of 8°, radiation quality N-60 and N-200, SCD of 100 cm and 300 cm, CWD of 2.2-50 cm, the variation of backscatter factor k_{MC} with CWD when the wall materials are; (a) brick, (b) ordinary concrete, (c) heavy concrete, (d) iron, and (e) lead

dosemeter installation wall backscatter factor with SCD, CWD, field size, and wall materials was investigated. For ordinary concrete material, the variation of backscatter factor with photon energy under different SCD and θ was verified, with a relative deviation between measured and simulated results within ±4.7 %. Results showed that the CWD and the size of the radiation field directly affected the measurement results. During the calibration process, the impact of scattered radiation can be reduced by adjusting the measurement distance and using appropriate beam apertures.

Finally, the variation of the backscatter factor with different wall scattering materials was studied using radiation qualities of N-60 and N-200 as examples. It was found that ordinary concrete and brick materials exhibited similar patterns of change, with a maximum backscatter factor not exceeding 1.35. For heavy concrete and lead materials, the backscatter factor significantly increased, near the energy region of the K absorption edge, because of characteristic X-rays. The maximum backscatter factor is 1.57 for heavy concrete at N-60, with CWD of 2.2 cm, and SCD of
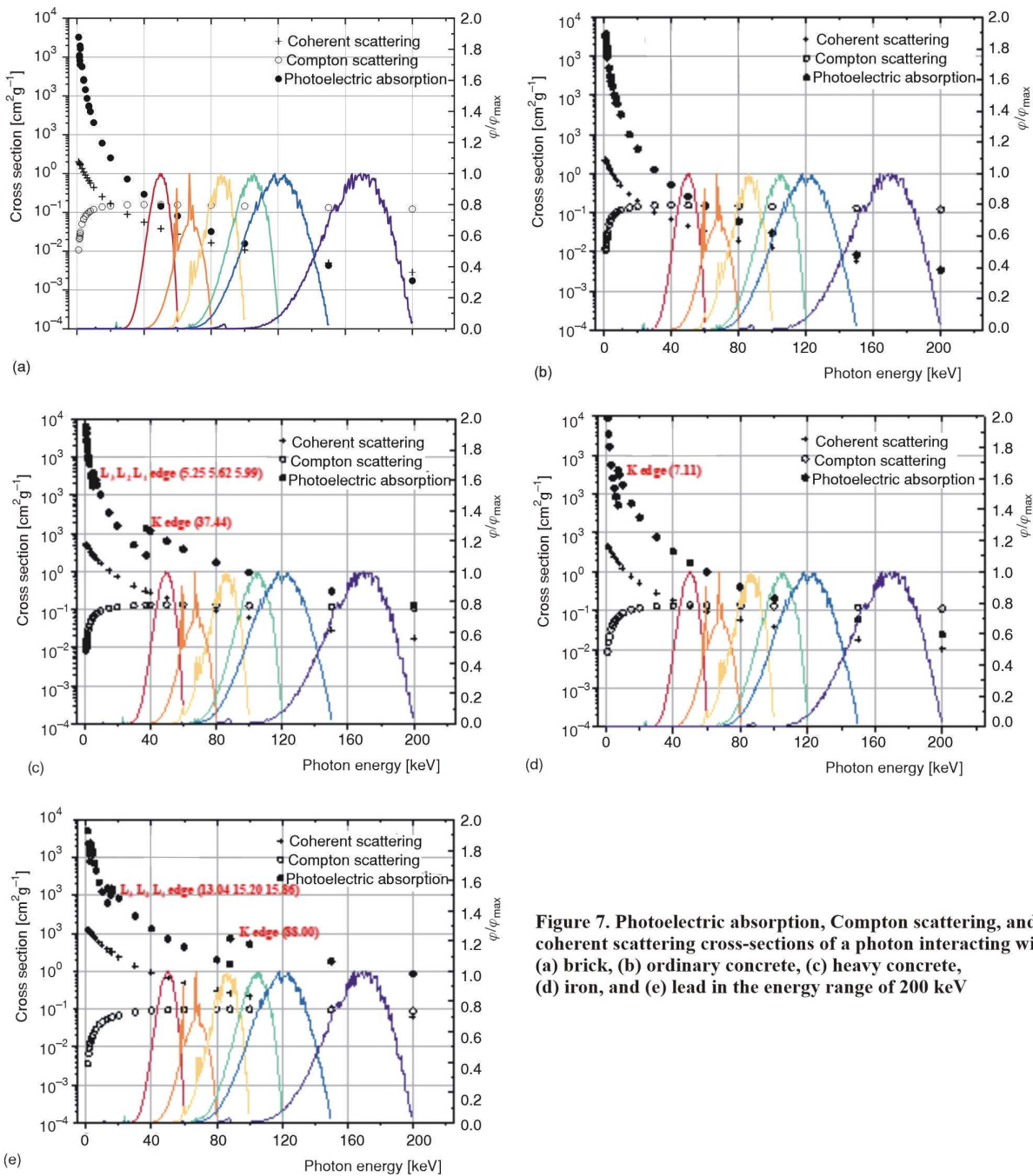
Figure 7. Photoelectric absorption, Compton scattering, and coherent scattering cross-sections of a photon interacting with; (a) brick, (b) ordinary concrete, (c) heavy concrete, (d) iron, and (e) lead in the energy range of 200 keV

300 cm. This research highlights the importance of considering wall materials, detector size, radiation field size, and photon energy in the process of *in-situ* calibration using mobile X-ray irradiation devices. The findings provide a solid theoretical basis for *in-situ* calibration and offer valuable data to support future studies.

AUTHORS' CONTRIBUTIONS

Y. Xu conducted experiments, simulated data acquisition, and manuscript writing, C. Luo analyzed and verified the data, Y. Huang and K. B. Jia made critical revisions to the manuscript, M. Lin and Y. T. Liu provided the research ideas and methods for the manuscript, as well as the experimental platform.
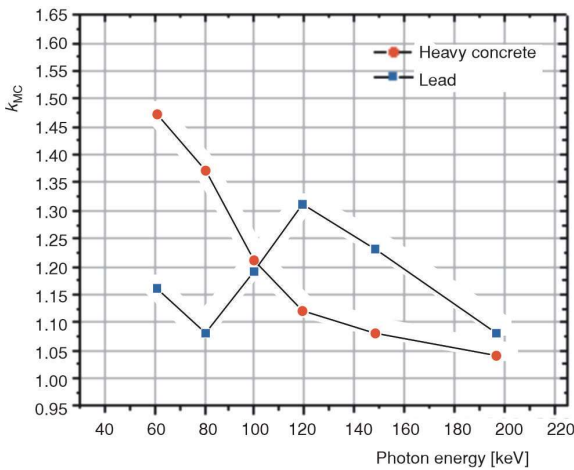
ORCID NO

Yang Xu: 0000-0001-6935-1376

Figure 8. The θ of 8°, radiation quality N-60 and N-200, SCD of 100 cm, CWD of 2.2 cm, the variation of backscatter factor with photon energy under heavy concrete and lead materials

REFERENCES

[1]   Živanović, M. Z., *et al.*, Comparison of Calibration Factors for Field-Class Dosimeters, *Nucl Technol Radiat, 37* (2022), 2, pp. 103-110

[2]   Wu, Y. C., *et al.*, Intercomparison of Environmental Gamma Radiation Dose Rate Measurements within the National Radiation Environmental Monitoring Network of China, *Radiation Protection Bulletin, 36* (2016), 1, pp. 1-9

[3]   Gostilo, V. V., *et al.*, Development of Nuclear Radiation Monitors for Radiation Early Warning Systems, *Nucl Technol Radiat, 37* (2022), 3, pp. 193-200

[4]   Xu, J. C., *et al.*, Analysis of Characteristic and Development Trend for Nuclear Power Plant Radiation Monitoring Instrument From System Design, *Nuclear Electronics & Detection Technology, 29* (2009), 5, pp. 1241-1247

[5]   ***, International Organization for Standardization, ISO 4037-1:2019, X and Gamma Reference Radiation for Calibrating Dosemeters and Doserate Meters and for Determining Their Response as a Function of Photon Energy-Part1: Radiation Characteristics and Production Methods, 2019

[6]   ***, International Organization for Standardization, ISO 4037-2:2019, X and Gamma Reference Radiation for Calibrating Dosemeters and Doserate Meters and for Determining Their Response as a Function of Photon Energy-Part2: Dosimetry for Radiation Protection over the Energy Ranges from 8 keV to 1.3MeV and 4MeV to 9MeV. (2019).

[7]   ***, International Organization for Standardization, ISO 4037-3:2019, X and Gamma Reference Radiation for Calibrating Dosemeters and Doserate Meters and for Determining Their Response as a Function of Photon Energy-Part3: Calibration of Area and Personal Dosemeters and the Measurement of Their Response as a Function of Energy and Angle of Incidence, 2019

[8]   ***, International Electrotechnical Commission, IEC 60846-1:2009, Radiation Protection Instrumentation - Ambient and/or Directional Dose Equivalent (Rate) Meters and/or Monitors for Beta, X and Gamma Radiation – Part 1: Portable Workplace and Environmental Meters and Monitors, 2009

[9]   Xu, Y., *et al.*, Optimization Design of Portable X-Ray Irradiation Device for *On-site* Calibration and Study of its Radiation Characteristics, *Radiation Protection, 41* (2021), 2, pp. 97-104

[10]   Wei, K. D., *et al.*, Study on the Establishment and Characteristics of Narrow-Series Radiation Quality of Mobile X-Ray Irradiation Device, *Journal of Astronautic Metrology and Measurement, 41* (2021), 5, pp. 50-56

[11]   ***, X-5 Monte Carlo Team, MCNP – A General Monte Carlo N-Particle Transport Code, Version 5. LA-CP-03-0245, LANL, 2003

[12]   ***, International Commission on Radiological Protection, ICRP Publication 74, Conversion Coefficients for Use in Radiological Protection Against External Radiation, 1996

[13]   Williams, R. G., Compendium of Material Composition Data for Radiation Transport Modeling, Office of Scientific & Technical Information Technical Reports, Richland, Washington, 2011

[14]   Xu, Y., *et al.*, Simulation Study on the Fraction of Environmental Scattered Radiation in Mobile X-ray Reference Radiation Field, *Nuclear Techniques, 44* (2021), 10, pp. 1-9

[15]   ***, XCOM: Photon Cross Sections Database, NIST Standard Reference Database 8 (XGAM), NIST Standard Reference Database Number 8, November 2010, https://www.nist.gov/pml/xcom-photon-crosssections-database. Accessed 1 Sept 2021

Јанг СЈУ, Чен ЛУО, Јен ХУАНГ, Кебин ЂА, Јуентао ЉУ, Мин ЛИН

ПРОУЧАВАЊЕ ФАКТОРА РЕФЛЕКСИЈЕ ОД ЗИДА У МОБИЛНОЈ *IN SITU* КАЛИБРАЦИЈИ РЕНДГЕНСКОГ ЗРАЧЕЊА

Овај рад фокусира се на *in situ* калибрацију монитора зрачења испитивањем промена фактора рефлексије. Развијен је мобилни уређај за рендгенско зрачење и утврђен је референтни ниво зрачења. Користећи Монте Карло методу, креиран је мерни модел *in situ* калибрације за проучавање фактора рефлексије на различитим растојањима и условима поља зрачења, за квалитет зрачења у распону од N-60~N-200. Верификована је тачност симулације, при чему релативно одступање између симулационих и експерименталних резултата није веће од ±4.7 %. Поред тога, симулирана је варијација фактора рефлексије са различитим растојањима између коморе и зида и материјала зида. Резултати показују да фактори рефлексије за све материјале опадају са повећањем удаљености коморе од зида. За конвенционални бетон, максимални фактор рефлексије у оквиру проучаваног енергетског опсега није прелазио 1.35. Важно је напоменути да за тежак бетон и олово, присуство K апсорпционих ивица може довести до наглог повећања расејаног зрачења.

Кључне речи: мобилан рендгенски уређај, in situ калибрација, керма у ваздуху, фактор рефлексије, Монте Карло